https://doi.org/10.5194/gmd-2020-327
Preprint. Discussion started: 29 October 2020

Geoscientific Model Development
Discussions

The Effects of Ocean Surface Waves on Global Forecast in CFS Modeling System v2.0

Ruizi Shi[1], Fanghua Xu[1], Li Liu[1], Zheng Fan[1], Hao Yu[1], Xiang Li[2] and Yunfei Zhang[2]

[1]Ministry of Education Key Laboratory for Earth System Modeling, and Department of Earth System Science, Tsinghua University, Beijing 100084, China

[2] Key Laboratory of Marine Hazards Forecasting, National Marine Environmental Forecasting Center, Ministry of Natural Resources, Beijing, 100081, China

Correspondence to: Fanghua Xu (fxu@mail.tsinghua.edu.cn)

Abstract. It has been well known that ocean surface gravity waves have enormous effects on physical processes at the atmosphere–ocean interface. However, the effects of surface waves on global forecast in several days are less studied. To investigate this, we incorporated the WAVEWATCH III model into the Climate Forecast System Model version 2.0 (CFS2.0), with the Chinese Community Coupler version 2.0 (C-Coupler2). Two major wave-related processes, the Langmuir mixing and the sea surface momentum roughness, were considered. Extensive comparisons were performed against in-situ buoys, satellite measurements and reanalysis data, to evaluate the influence of the two processes on the forecast of sea surface temperature, mixed layer depth, significant wave height, and 10-m wind speed. A series of 7-day simulations demonstrate that the newly developed atmosphere-ocean-wave coupling system could improve the CFS global forecast. The Langmuir mixing parameterization could increase the vertical movement of water and effectively reduce the warm bias of sea surface temperature and shallow bias of mixed layer depth in the Antarctic circumpolar current in austral summer, whereas the significant wave height and 10-m wind speed are insensitive to it. On the other hand, the modified momentum roughness length could significantly reduce the overestimated 10-m wind speed and significant wave height in mid-high latitudes. This is because the enhanced frictional dissipation at high wind speed could

https://doi.org/10.5194/gmd-2020-327
Preprint. Discussion started: 29 October 2020

Geoscientific Model Development Discussions

reduce 10-m wind speed and consequently decrease the significant wave height. But its effect on the temperature structure in upper ocean is less obvious.

1 Introduction

Ocean surface gravity waves play an important role in modifying physical processes at the atmosphere–ocean interface, which can influence momentum, heat, and moisture fluxes across the air-sea interface (Li and Garrett 1997; Taylor and Yelland, 2001; Moon et al., 2004; Belcher et al., 2012; Moum and Smyth, 2019). For instance, ocean surface waves can modify the ocean surface roughness to influence the marine atmospheric boundary layer and thus change the momentum, latent heat, and sensible heat transfer (Taylor and Yelland, 2001; Moon et al., 2004). The breaking waves inject turbulent kinetic energy in the upper ocean, which can enhance the mixing process (Terray et al. 1996). Nonbreaking surface waves can also affect mixing in the upper ocean by adding a wave-related Reynolds stress (Qiao et al., 2004). The wave-related Stokes drift interacts with the Coriolis force and produces the Coriolis-Stokes force (Hasselmann 1970). The shear of Stokes drift is a critical reason for the generation of Langmuir circulation, which could significantly deepen the mixed layer by strong vertical mixing process both at climate scale (Li and Garrett 1997; Belcher et al., 2012) and at weather scale (Kukulka et al., 2009). If sea ice is present, the interaction of wave, ocean and atmosphere is further complicated (Kohout and Meylan, 2008; Squire et al., 2009).

As Fox-Kemper et al. (2019) expected, the improvement to atmosphere-ocean coupling with a better presentation of the effects of surface gravity waves, is one of the challenges and focuses in ocean modeling for the next decade. Regional coupled models were developed to study tropical cyclones, storm surge and other coastal processes at small or medium scales (e.g. Prakash et al., 2018; Ricchi et al., 2017;

https://doi.org/10.5194/gmd-2020-327
Preprint. Discussion started: 29 October 2020

Geoscientific Model Development Discussions
Open Access
EGU

Pianezze et al., 2018; Wu et al., 2019). The Coupled Ocean-Atmosphere-Wave-Sediment Transport Modeling System (COAWST) developed by Warner et al. (2010) is one of well-known fully-coupled models, which includes effects of wave-state-dependent ocean surface roughness, radiation stress, bottom stress and Stokes drift-related processes. The COAWST has been well applied in various locations such as the South China Sea (Sun et al., 2019; Wu et al., 2019), Bay of Bengal (Prakash et al., 2018) and Mediterranean (Ricchi et al., 2017). On the other hand, the coupled models with a wave component at global scale were primarily developed for long-term climate research (e.g. Qiao et al. 2010; Breivik et al. 2015; Chune, et al. 2018; Fan et al., 2012; Fan and Griffies, 2014; Li et al. 2016, 2017). The effects of waves on short term forecast at global scale have been considered negligible for long time. Since the impact of wave-related processes is important not only for the synoptic processes but also for the frequent interactions at multiple spatial scales as aforementioned, it is of great interest to investigate the effects of surface ocean waves on short-term forecast in a global atmosphere-ocean-wave system with suitable presentations of wave-related processes.

To realize a fully-coupled modeling system, establishing suitable connections between the wave component and the atmosphere/ocean component are crucial. In coupled systems, commonly the atmosphere and ocean components provide 10-m winds and surface currents, sometimes with other variables such as sea surface temperature and water depth, to the wave model as forcing fields (Chen et al. 2007; Warner et al. 2010; Breivik et al. 2015; Li et al. 2016; Pianezze et al., 2018). Compared to a single wave model, in which the inputted reanalysis datasets usually have an interval more than 3 hours, the forcing fields in the wave component have a finer time interval (Fan et al., 2012). Meanwhile, the wave component sends wave parameters, such as wave length, period and significant wave height, to the atmosphere and ocean components. These wave parameters could be used in various wave-related parameterizations. In this study, we coupled the WAVEWATCH III to the Climate Forecast System Model (CFS) using the Chinese Community Coupler version 2.0 (C-Coupler2). We mainly considered two effects induced by waves at the ocean-atmosphere interface, surface roughness and Langmuir cells induced mixing. This is because both processes have strong influences on momentum and energy fluxes across the air-sea interface and could effectively improve the simulation results (e.g. Fan et al., 2012; Fan and Griffies, 2014; Li et al. 2016, 2017). Four series of 7-day forecasts were produced with this system. The performance of the system was then compared with observations and reanalysis data. Sensitivity experiments with various wave parameterizations were carried out to evaluate the contributions of surface roughness and Langmuir mixing to the changes of atmosphere and ocean. In addition, the performance of various wave parameterizations was evaluated as well. The analysis is structured as follows: methods and a set of experiments with various parameterizations are described in Section 2; the observation and reanalysis data are introduced in Section 3, and the results of experiments are evaluated against these available data in Section 4; a summary and discussion follow in Section 5.

2 Methods and Experiments

2.1 Coupling WAVEWATCH III with CFS2.0

The version 5.16 of WAVEWATCH III (WW3; WAVEWATCH III Development Group, 2016) developed by the National Oceanic and Atmospheric Administration/National Centers for Environmental Prediction (NOAA/NCEP) has been incorporated into the Climate Forecast System Model, version 2.0 (CFS2.0; Saha et al., 2014) as a new model component. The latitude range of WW3 is 78°S–78°N with a spatial resolution of 1/3°; the frequency range is 0.04118-0.4056Hz and the total number of frequencies is 25; the number of wave directions is 24 with a resolution of 15°; the maximum global time step is 450

https://doi.org/10.5194/gmd-2020-327
Preprint. Discussion started: 29 October 2020

s and the minimum source term time step is 300 s. The CFS contains two components, the global forecasting system (GFS; details about the GFS are available at http://www.emc.ncep.noaa.gov/GFS/doc.php) as the atmosphere component and the modular ocean model version 4 (MOM4; Griffies et al., 2004) as the ocean component. The MOM4 is integrated on a nominal 0.5° horizontal grid with enhanced horizontal resolution in the tropics, and has 40 vertical levels; the vertical spacing is 10 m in the upper 225 m, and then increases in unequal intervals to the bottom at 4478.5 m. The GFS uses a spectral triangular truncation of 126 waves (T126) in the horizontal, which is equivalent to a grid resolution of nearly 100 km, and 64 sigma-pressure hybrid layers in the vertical. The time steps of both MOM4 and GFS are 180 s.

This coupled system uses the Chinese Community Coupler version 2.0 (C-Coupler2; Liu et al., 2018) for interpolating and passing variables between its atmosphere, ocean, and wave components, to guarantee each component receives inputs and supplies outputs on its own grid. The C-Coupler2 is a common, flexible and user-friendly coupler, which contains dynamic 3-D coupling system and enables variables to remain conserved after interpolation. The variables are exchanged every other time step, which in atmosphere and ocean components is 180 s, and in wave component is 450 s.

A schematic diagram of the coupled atmosphere-ocean-wave system is shown in Fig. 1. As illustrated, WW3 is two-way coupled with MOM4 and GFS, through the C-Coupler2. WW3 is forced by 10-m wind from GFS and sea surface current from MOM4, and then generates and evolves the wave action density spectrum. Meanwhile, the momentum roughness length is passed to GFS from WW3 (see section 2.3), and the surface Stokes drift velocity is passed to MOM4 (see section 2.2). In this study, both the CFS and WW3 use warm boots; the daily initial fields at 00:00 for CFS are generated by the real time operational Climate Data Assimilation System (CDAS; Kalnay et al., 1996), downloaded from the CFS

https://doi.org/10.5194/gmd-2020-327
Preprint. Discussion started: 29 October 2020

Geoscientific Model Development Discussions
Open Access

official website (http://nomads.ncep.noaa.gov/pub/data/nccf/com/cfs/prod). To get initial conditions for WW3, a single WW3 model is set up synchronously (see section 2.4).

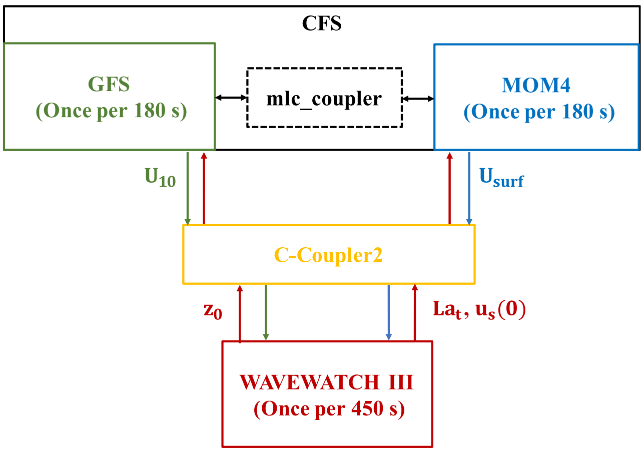

Figure 1. A schematic diagram of the atmosphere-ocean-wave coupled modeling system. *The arrows* indicate the coupled variables that are passed between the model components. In the diagram, z_0, La_t, $u_s(0)$, U_{10}, and U_{surf} are momentum roughness length, turbulent Langmuir number, surface Stokes drift velocity, 10-m wind and surface current, respectively.

2.2 Parameterizations of Langmuir Mixing

2.2.1 McWilliams and Sullivan (2000) Parameterization

McWilliams and Sullivan (2000) improved the turbulent velocity scale W in KPP by introducing an enhancement factor ε, to account for both boundary layer depth changes and nonlocal mixing by Langmuir turbulence. In their work, they indicated W (W=ku_*/ϕ, where u_* is the surface friction velocity, ϕ is the dimensionless flux profile, and *k*=0.4 is the von Kármán constant) varies in proportion to the turbulent Langmuir number, that is,

$$\mathrm{W} = \frac{ku_*}{\phi}\varepsilon, \qquad (1)$$

$$\varepsilon = \sqrt{1 + 0.08La_t^{-4}}, \qquad (2)$$

https://doi.org/10.5194/gmd-2020-327
Preprint. Discussion started: 29 October 2020

Geoscientific Model Development Discussions

where La_{t} is the turbulent Langmuir number. And La_{t} is defined as

$$La_{\mathrm{t}} = \sqrt{\frac{u_*}{|u_s(0)|}}, \tag{3}$$

with $u_s(0)$ is the surface Stokes drift velocity. Hereafter, we refer to this parameterization as MS2K. Furthermore, the enhanced W will influence the calculation of boundary layer depth. In KPP the boundary layer depth is determined as the smallest depth at which the bulk Richardson number equals the critical value $Ri_{\mathrm{cr}} = 0.3$, that is,

$$Ri_b(h) = \frac{gh[\rho_r - \rho(h)]}{\rho_0[|u_r - u(h)|^2 + W^2]} = Ri_{\mathrm{cr}}, \tag{4}$$

where g is acceleration of gravity, ρ is density, u is velocity, ρ_r is surface density, u_r is surface velocity, ρ_0 is an average value and h is the boundary layer depth. Hence, when W is enhanced, the boundary layer depth h is deepened accordingly.

2.2.2 Van et al. (2012) Parameterization

Based on the work of McWilliams and Sullivan (2000), Van et al. (2012) proposed a different formula for the enhancement factor, and a projected Langmuir number considering the misalignment of winds and waves. They suggested a projected Langmuir number,

$$La_{\mathrm{proj}} = \sqrt{\frac{u_* \cos(\alpha)}{|u_s(0)|\cos(\theta_{ww} - \alpha)}}, \tag{5}$$

$$\alpha \approx tan^{-1}\left[\frac{sin\theta_{ww}}{\frac{u_*}{u_s(0)k}\ln\left(\left|\frac{h}{Z_1}\right|\right) + cos\theta_{ww}}\right]. \tag{6}$$

Here α is the angle between wind and Langmuir cell, θ_{ww} is the angle between Stokes drift and wind, and Z_1 is the four times of the significant wave height. In this case, Van et al. (2012) suggested the form of ε should be

https://doi.org/10.5194/gmd-2020-327
Preprint. Discussion started: 29 October 2020

$$\varepsilon = |cos\alpha| \sqrt{1 + (3.1La_{\mathrm{proj}})^{-2} + (5.4La_{\mathrm{proj}})^{-4}}. \quad (7)$$

In the work of Li et al. (2016) these parameterizations corresponding to alignment and misalignment of winds and waves (referred to as VR12-AL with $\alpha \equiv 0$ and VR12-MA with α not zero) were employed in a coupled global climate model. As Li et al. (2016) illustrated, the difference between the effects of VR12-AL and VR12-MA is not significant, owing to the limitation of coarse resolution which cannot accurately represent the refraction by coasts and current features. Besides, the VR12-MA will certainly increase the runtime due to increased variables to be transferred from wave to ocean. Considering all above, we employ the VR12-AL parameterization. In VR12-AL, the La_{proj} (Eqn. 5) reduces to La_{t} (Eqn. 3).

2.3 Parameterizations of Momentum Roughness

In a coupled model, the estimates of momentum, latent heat, and sensible heat fluxes between atmosphere and ocean are critically important. These fluxes are in part determined by surface roughness length, which can be converted to drag coefficient.

In GFS, the Charnock relationship (Charnock, 1955) is used to parameterize the momentum roughness length as

$$z_{ch} = \frac{z_0 g}{u_*^2}. \quad (8)$$

Here z_0 is the roughness length, and $z_{ch} = 0.014$ is the constant Charnock number. The corresponding scatterplot of z_0 in GFS versus 10-m wind speed is shown in Fig.2 (black dots). The z_0 in GFS increases relatively slowly with increasing wind speed, especially at high winds.

https://doi.org/10.5194/gmd-2020-327
Preprint. Discussion started: 29 October 2020

Geoscientific Model Development
Discussions

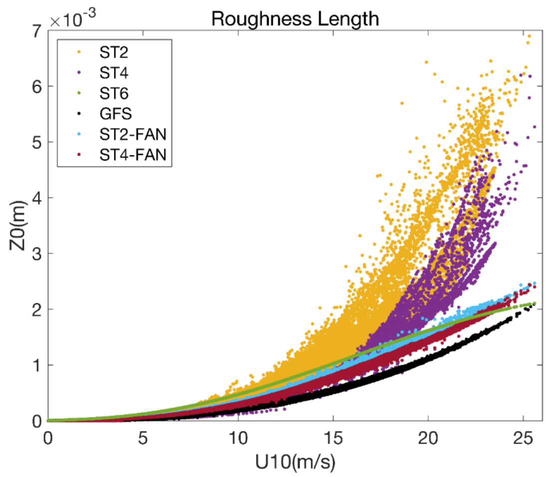

Figure 2. Scatterplot of momentum roughness length z_0 (m) in various source term packages versus 10-m wind speed (m/s).

In WW3, input of momentum and energy by wind, and dissipation for wave-ocean interaction are two important terms (combined as input-dissipation source term) in the energy balance equation (WAVEWATCH III Development Group, 2016). Several different packages to calculate the input-dissipation source term (ST) are offered in the WW3 version 5.16, and the most commonly used ones are ST2 (Tolman and Chalikov, 1996), ST3 (Janssen, 2004; Bidlot, 2012), ST4 (Ardhuin et al., 2010), and ST6 (Zieger et al., 2015). In ST4 package, wind speed is assumed to satisfy the traditional logarithmic profile in the neutral boundary layer

$$U_{10} = \frac{u_*}{k}\log(\frac{z_{10}}{z_0}), \qquad (9)$$

where U_{10} is 10-m wind speed, and z_{10} is the corresponding height (10 m). The same relationship is also used in ST2 package (Tolman and Chalikov, 1996). And the roughness length z_0 is obtained from this relationship in ST4 and ST2 (purple and yellow dots in Fig.2). Fan et al., (2012) indicated that the z_0 in ST2 increases rapidly with wind speed at high winds and results in the fast-increasing drag coefficient, which is inconsistent with the drag coefficient leveling off for extremely high wind speed in

https://doi.org/10.5194/gmd-2020-327
Preprint. Discussion started: 29 October 2020

observation and laboratory experiments. Although the rising trend of ST4 is slightly slower than that of ST2, the rapid increase of z_0 at high winds still exists. For this reason, the ST6 calibrated with flux parameterization FLX4 was proposed by Zieger et al. (2015) and accounts for the saturation of the sea drag at high wind speeds (green dots in Fig.2). However, the drag coefficient in ST6 is calculated by wind speed only without wave state considered, and this does not accord with the fact.

To solve these problems, Fan et al., (2012) suggested an improved parameterization for z_0 in ST2 (referred to as ST2-FAN). In ST2-FAN, z_0 is calculated by the improved Charnock relationship, in which the Charnock number is not a constant but depends on the wave state (Moon et al., 2004), that is,

$$\frac{z_0 g}{u_*^2} = a\left(\frac{c_{pi}}{u_*}\right)^b, \tag{10}$$

$$a = \frac{0.023}{1.0568^{U_{10}}}, b = 0.012U_{10}, \tag{11}$$

where c_{pi} is the phase speed of dominant wind-forced waves.

In this study, we chose the ST4 package to calculate the input and dissipation term, since ST4 has shown the best performance in the simulation of significant wave height (SWH) at global scale (compared in section 2.4), which is consistent with the study of Stopa et al (2016). Fan et al. (2012)'s parameterization was then applied in ST4 (referred to as ST4-FAN) to obtain new z_0. The estimates of z_0 from ST2-FAN and ST4-FAN are shown in blue and dark red dots of Fig.2, respectively. The fast-rising trend of z_0 at high wind speed is obviously restrained. And z_0 from ST4-FAN is generally smaller than that from ST2-FAN.

2.4 Initialization of WAVEWATCH III

The initial wave fields were generated from the 10-day simulations starting from rest in a single WW3 model. To minimize the biases of the initial wave fields, we ran simulations with ST2, ST3, ST4, and

https://doi.org/10.5194/gmd-2020-327
Preprint. Discussion started: 29 October 2020

Geoscientific Model Development
Discussions
Open Access

ST6 source terms respectively, and compared the results. Besides, two 10-m wind datasets were used and compared as the wave model forcing, namely the Cross-Calibrated Multi-Platform (CCMP; Atlas et al., 2011) data and the fifth generation European Centre for Medium-Range Weather Forecasts (ECMWF) Reanalysis (ERA5; Hersbach and Dee, 2016) data. After comparisons, the ST4 source term with ERA5 wind forcing, which generated the minimum SWH bias (Table S1 in the supplementary), was applied to generate initial wave fields for all experiments listed in Table 1.

Table 1. List of Numerical Experiments

Experiments	**WW3 to MOM4**	**WW3 to GFS**
CTRL	None	None
VR12-AL-ONLY	VR12-AL parameterization	None
Z0-ONLY	None	z_0 from ST4
VR12-AL-Z0	VR12-AL parameterization	z_0 from ST4
MS2K-Z0	MS2K parameterization	z_0 from ST4
VR12-AL-Z0-FAN	VR12-AL parameterization	z_0 from ST4-FAN

2.5 Set of Experiments

A series of numerical experiments was conducted to evaluate the effects of Langmuir mixing parameterizations and momentum roughness lengths on the ocean and atmosphere in four 7-day periods, January 3 to 10, 2017, July 1 to 8, 2018, August 3 to 10, 2018, and January 1 to 8, 2019.

The reference experiment (CTRL) is a one-way coupled experiment, in which GFS and MOM4 provide 10-m wind and sea surface current to WW3, whereas no variables transmission from WW3 to CFS. The results of CFS in CTRL are consistent with the corresponding CFS Reanalysis data (Saha et al., 2010).

For each time period, five sensitivity experiments were carried out. The first is VR12-AL-ONLY simulation, in which the VR12-AL parameterization is added in MOM4. The second is Z0-ONLY

https://doi.org/10.5194/gmd-2020-327
Preprint. Discussion started: 29 October 2020

simulation, in which the original z_0 in GFS is replaced by z_0 from WW3 ST4 source term. Then based on the VR12-AL-ONLY simulation, the VR12-AL-Z0 simulation is performed with z_0 from WW3 ST4 source term in GFS. The MS2K-Z0 simulation is similar to the VR12-AL-Z0 simulation, but using the MS2K instead of VR12-AL. The last experiment is the VR12-AL-Z0-FAN, in which z_0 is generated by the ST4-FAN source term in WW3 and other settings remain the same as VR12-AL-Z0.

3 Data

Sea surface temperature (SST), profiling temperature and salinity, 10-m wind speed (WSP10), and significant wave height (SWH) from observations and reanalysis datasets are used to evaluate the simulation results.

The daily average satellite Optimum Interpolation SST (OISST) data is obtained from the National Oceanic and Atmospheric Administration (NOAA), with 0.25°×0.25° resolution (Reynolds et al., 2007; https://www.ncdc.noaa.gov/oisst). The global Argo observational profiles of temperature and salinity (Li et al., 2019) is from China Argo Real-time Data Center (www.argo.org.cn). The fifth generation European Centre for Medium-Range Weather Forecasts (ECMWF) Reanalysis (ERA5) datasets of WSP10 and SWH with a spatial resolution of 0.5° and a temporal resolution of 1 hour are also used (Hersbach and Dee, 2016; https://cds.climate.copernicus.eu/cdsapp#!/dataset/ reanalysis-era5-single-levels). Additionally, the WSP10 and SWH observations from the available National Data Buoy Center (NDBC) buoy data (https://www.ndbc.noaa.gov), and the along-track SWH from Jason-3 satellite measurements (https://aviso-data-center.cnes.fr) Geophysical Data Record (GDR) with precise orbit and an orbital velocity of 7.2 km/s are applied for comparison purposes.

https://doi.org/10.5194/gmd-2020-327
Preprint. Discussion started: 29 October 2020

Geoscientific Model Development Discussions
Open Access
EGU

4 Results

4.1 SST and Mixed Layer Depth (MLD)

The application of Langmuir mixing parameterization in KPP can change the SST, because the modified turbulent vertical velocity scale enhances surface ocean mixing, which tends to reduce SST. In the study, the distribution pattern of biases is almost unchanged within 7 days. But the magnitude of the biases slightly increases with time, and the influences of parameterizations also become more obvious. Without loss of generality, we compared the distributions of SST on the 4th day as the intermediate state, and the similar distributions on the last day are also shown in Figs. S1&S2 of the supplementary. Figure 3 and Figure 4 show the distribution maps of daily average SST in CTRL (Fig.3a&4a), its bias (Fig.3b&4b) and percentage absolute difference of the bias from experiments versus the CTRL (Fig. 3c-g and Fig. 4c-g), on January 7, 2017 and August 7, 2018 (the 96th-120th hours), respectively. Here the bias is defined as SST in CTRL minus OISST. And to highlight the differences of other experiments versus the CTRL, the percentage absolute differences (PAD) of the bias are computed as $\mathrm{PAD} = \frac{|\hat{y_s}-y|-|\hat{y_c}-y|}{|y|} \times 100\%$, where y is OISST, $\hat{y_c}$ is simulated SST in CTRL and $\hat{y_s}$ is simulated SST in other experiments (Fig. 3c-g and Fig. 4c-g). A negative value of PAD indicates that the error is smaller compared to CTRL, and vice versa.

https://doi.org/10.5194/gmd-2020-327
Preprint. Discussion started: 29 October 2020

Geoscientific Model Development
Discussions

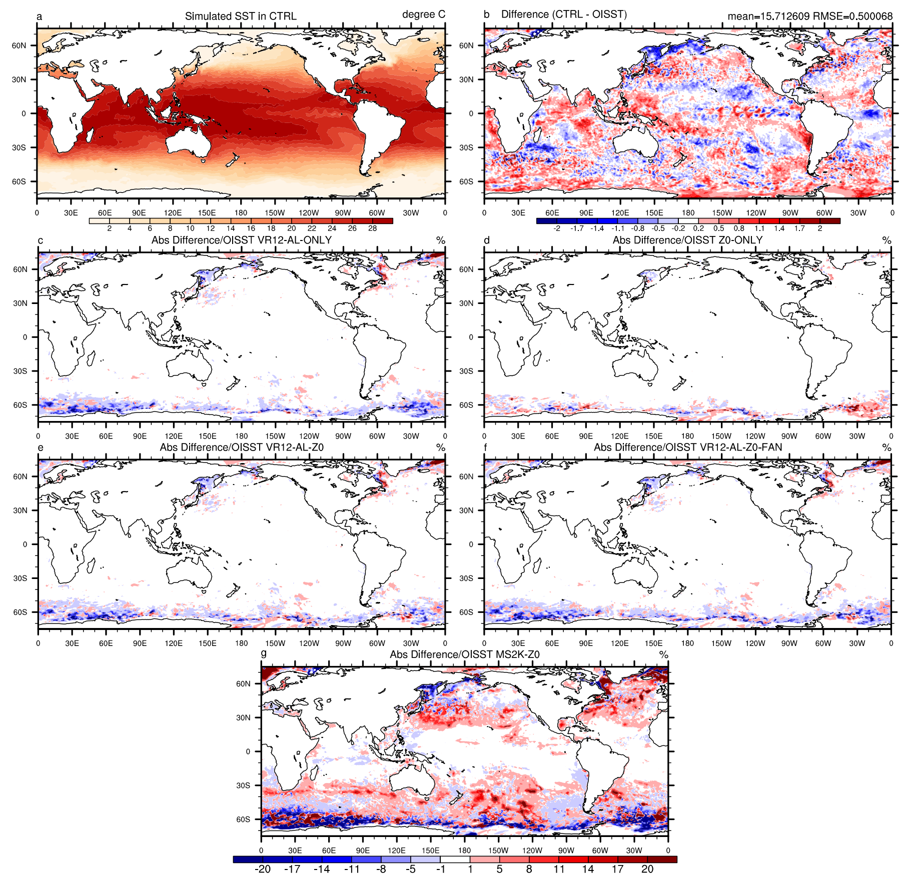

Figure 3. The daily average SST (℃) in CTRL, its bias in CTRL and percentage absolute difference of bias on January 7, 2017: **a** the SST in CTRL, **b** the SST bias between CTRL and OISST (CTRL minus OISST), **c/d/e/f/g** the percentage absolute difference between VR12-AL-ONLY/Z0-ONLY/VR12-AL-Z0/VR12-AL-Z0-FAN/MS2K-Z0 and CTRL. The absolute difference is a percentage computed as $\mathrm{PAD} = \frac{|\hat{y}_s - y| - |\hat{y}_c - y|}{|y|} \times 100\%$, where y is OISST, $\hat{y}_c$ is simulated SST in CTRL and $\hat{y}_s$ is simulated SST in other experiments, so a negative value means that the error is smaller than that of CTRL, and vice versa.

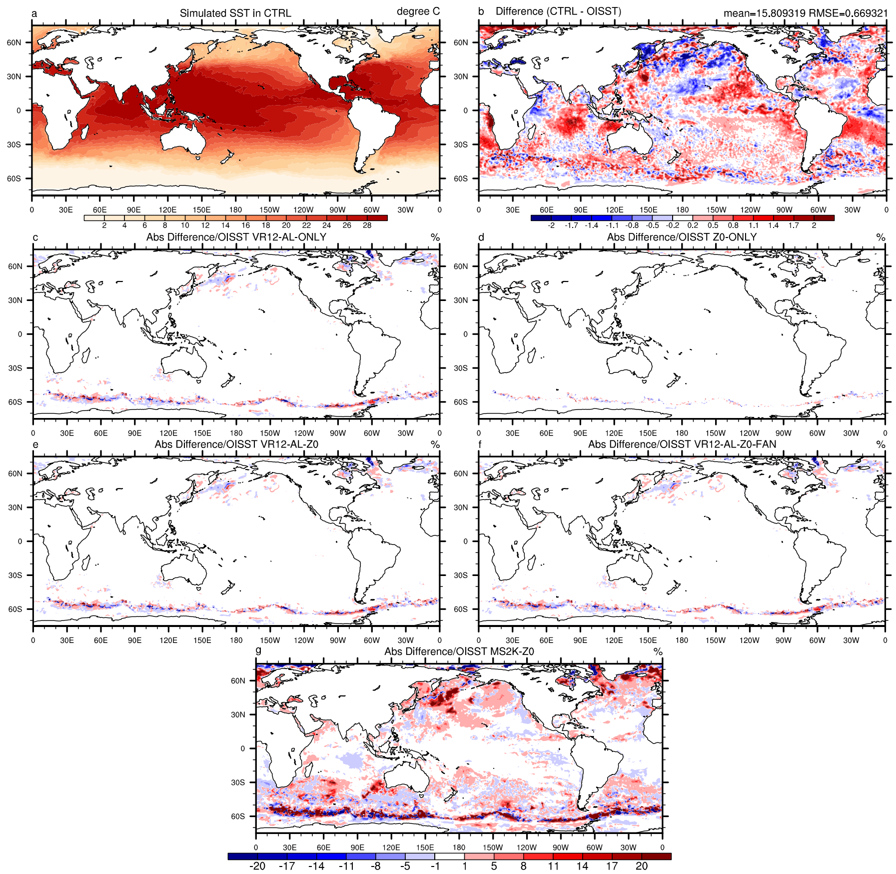

Figure 4. As Fig. 3, but for the daily average SST (℃) in CTRL, its bias in CTRL and absolute difference of bias on August 7, 2018.

As shown in Fig. 3a and 3b, the global mean SST in CTRL is approximately 15.71℃, which is close to the mean SST from OISST (approximately 15.22℃), and the average RMSE is about 0.50℃ in CTRL. The simulated SST is generally overestimated, and the large biases (>1.10℃) are mainly distributed at locations with active mesoscale vortices and frontal instability, such as the Kuroshio extension, the Peruvian upwelling, the Gulf Stream and the Antarctic Circumpolar Current (ACC; Fig. 3b). The Langmuir mixing can enhance the vertical turbulent velocity, and thus after introducing it the simulations should cool the surface waters and reduce warm biases in locations where Stokes drift related turbulence

https://doi.org/10.5194/gmd-2020-327
Preprint. Discussion started: 29 October 2020

kinetic energy is large (Belcher et al., 2012; Li et al. 2016). The warm bias of SST in VR12-AL-ONLY (Fig. 3c) is clearly decreased near the ACC, because of the strong Langmuir mixing. More than 5% bias reduction is achieved. The SST estimates are also improved by 5-11% in the Okhotsk Sea and the Bering Sea. But there is no clear change elsewhere. This is consistent with the distribution of relatively high SWH (Fig. 6a). In Fig. 3d, the SST improvements vanish, whereas in Fig. 3e and 3f the bias distributions are almost identical to Fig. 3c, indicating that the SST is insensitive to the change of surface roughness (z_0). In contrast, the biases from MS2K-Z0 (Fig. 3g) get worse in general, due to too much mixing induced by MS2K parameterization, which has cooled down the surface ocean greatly. As a result, although the warm bias in ACC is greatly reduced, the cold bias is enhanced in mid latitudes (Fig. 3g). Compared to the simulations in January, the simulations with VR12-AL parameterization in August show less improvements, especially in ACC, where the SST bias even partially increases (Fig. 4c, e, f) because of the reduced warm bias during austral winter in the south of 50°S (Fig. 4b). These results are consistent with the studies of Belcher et al. (2012) and Li et al. (2016), which indicated that the improvements of simulation by Langmuir mixing parameterizations in Southern Ocean are obvious mainly in austral summer but not winter. To examine the robustness of these variations, two tests from January 1 to 8, 2019 and from July 1 to 8, 2018 were conducted. The results are in good agreement with the previous simulations (Figs. S7&S8 in the supplementary). Similarly, the SST in August also becomes too cold in MS2K-Z0 (Fig. 4g), especially in the mid latitude regions of the Northern Hemisphere, where the SST is already underestimated in CTRL (Fig. 4b).

In order to further evaluate the direct effect of Langmuir mixing parameterizations, we compared the mixed layer depth (MLD) of all experiments with that of Argo profiles, since MLD could be deepened by the Langmuir mixing. The simulated temperature and salinity were interpolated onto the positions of

https://doi.org/10.5194/gmd-2020-327
Preprint. Discussion started: 29 October 2020

Argo profiles at the nearest time. The MLD was then estimated as the depth where the change of potential density reaches the value corresponding to a 0.2℃ decrease of potential temperature with unchanged salinity from surface (de Boyer Montégut et al., 2004). Considering the less improvements to the SST simulation by Langmuir mixing in August than in January, here we only compared the results of MLD in January, 2017. Comparisons of the MLDs between numerical experiments and Argo data in the ACC (0-360°E, 45-78°S) are shown in Fig. 5. Both the MS2K (dark red) and VR12-AL (yellow, blue and green) parameterizations lead to deepened MLD, compared to CTRL (orange). Noticeably, too much mixing introduced by MS2K parameterization results in the over-deepening of MLD. Considered the enhanced mixing effect resulted by Langmuir turbulence, when the simulated MLD in CTRL is shallower than observation (black), the bias is reduced in VR12-AL, such as the period from 6:00 on January 9 to 0:00 on January 10. However, when the simulated MLD in CTRL is overestimated, application of VR12-AL parameterization tends to increase the bias on the contrary, such as 0:00 on January 9. All in all, the biases of MLDs are reduced by Langmuir mixing. In addition, similar to the SST simulations, the differences of MLDs generated by different z_0 in VR12-AL-ONLY (yellow), VR12-AL-Z0 (blue) and VR12-AL-Z0-FAN (green) are quite few, indicating that the effect of surface roughness on upper ocean is not significant. This is also consistent with the fact that the result of Z0-ONLY (purple) has little difference with CTRL.

https://doi.org/10.5194/gmd-2020-327
Preprint. Discussion started: 29 October 2020

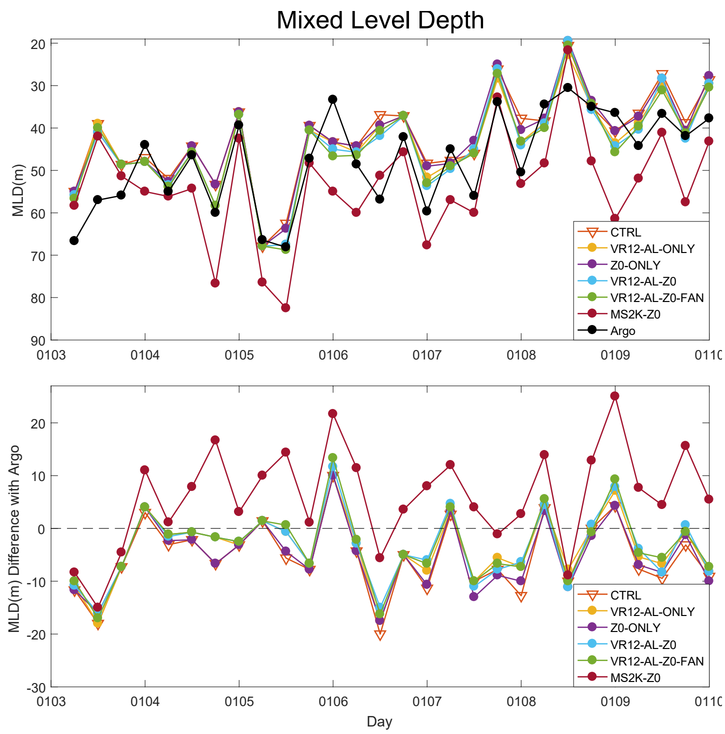

Figure 5. The time series of domain-averaged (0-360°E, 45-78°S) mixed layer depth (MLD; m; upper panel) and MLD bias versus Argo profile data (simulations minus Argo; lower panel). The time intervals are 6 hours.

4.2 Significant Wave Height (SWH) and Wind Speed at 10 m (WSP10)

To evaluate the performance of the wave simulation, the simulated SWHs were compared with Jason-3 GDR along-track quality-checked altimeter measurements and the ERA5 reanalysis data. Here we compared the Jason-3 data and simulations at 00:00 (the Jason-3 data within 20 min from 00:00 were applied), and interpolated the simulated SWHs at 00:00 onto the satellite orbit. The 7-day averaged SWH correlation coefficients, skill scores and RMSEs from 00:00 on Jan 3, 2017 to 00:00 on Jan 10, 2017 are documented in Table 2. Compared with CTRL, experiments with coupled z_0 show improvements to the SWH simulation, especially the VR12-AL-Z0-FAN. Although the improvements are not quite large, because those are the global average results, whereas the significant improvements mainly distribute in

https://doi.org/10.5194/gmd-2020-327
Preprint. Discussion started: 29 October 2020

the mid-high latitudes (Fig.6&7). The best results (with the highest correlation coefficient, the lowest RMSE and the highest skill score) in 6 experiments are marked in bold, all of which are from VR12-AL-Z0-FAN. Compared with CTRL, the RMSE in VR12-AL-Z0-FAN reduces 5.0%. In addition, we also calculated the difference between Jason-3 data and ERA5 reanalysis data (Table 2). The small bias suggests that the ERA5 data is reliable for comparison with the global distribution of simulations. And remarkably, the results of VR12-AL-Z0-FAN are close to ERA5. In the simulation starting from Aug 3, 2018, the correlation coefficient, skill score and RMSE of CTRL are 0.79, 0.86 and 0.68, and those of ERA5 are 0.88, 0.93 and 0.43. The difference between CTRL and ERA5 is larger, so there is more potential for improvement. Similarly, the best results in 6 experiments are still from VR12-AL-Z0-FAN, of which the RMSE is 0.61 and reduces 10.0%.

Table 2. 7-day Averaged Correlation Coefficient, RMSE and Skill Score of SWH in Simulations and ERA5 versus the Jason-3 Observation from 00:00 on Jan 3, 2017 to 00:00 on Jan 10, 2017. *Bold marks* represent the highest correlation coefficient, the lowest RMSE and the highest skill score (except ERA5); the RMSE and skill score (SS) are calculated as RMSE=$\sqrt{\sum_{i=1}^{n}(\hat{y}_i - y_i)^2/n}$ and SS=$1 - \frac{\sum_{i=1}^{n}(\hat{y}_i - y_i)^2}{\sum_{i=1}^{n}(|\hat{y}_i - \bar{y}_i| + |y_i - \bar{y}_i|)^2}$, respectively, where $\hat{y}_i$ is simulated value or ERA5 data, y_i is Jason-3 observation and $\bar{y}_i$ is the average, i=1,n and n is the total number of measurements in the Jason-3 orbit.

	Correlation Coefficient (P<0.01)	**RMSE**	**Skill Score**
CTRL	0.85	0.60	0.91
VR12-AL-ONLY	0.85	0.61	0.90
Z0-ONLY	0.85	0.58	0.91
VR12-AL-Z0	0.85	0.58	0.91
MS2K-Z0	0.82	0.60	0.89
VR12-AL-Z0-FAN	**0.86**	**0.57**	**0.92**
ERA5	0.87	0.51	0.92

To further investigate the effect of wave-related processes on the simulated distribution of SWH biases, we also compared the simulated SWH with the ERA5 data. Figure 6 and Figure 7 show the distributions of SWHs in CTRL (Fig.6a&7a), its bias (Fig.6b&7b) and percentage absolute difference of bias from experiments versus the CTRL (Fig. 6c-g and Fig. 7c-g) at 00:00 on January 7, 2017 and August 7, 2018 (the 96th hour), respectively. On January 7, 2017, the global mean SWH in CTRL is approximately 2.50 m, which is higher than the mean SWH from ERA5 (approximately 2.31 m). The average RMSE is about 0.48 m in CTRL. Large biases (> 1.0 m) appear in the ACC area and the mid-high latitudes of the Northern Hemisphere (Fig.6a&b). On August 7, 2018, the global mean SWH in CTRL is approximately 2.65 m and higher than that from ERA5 (approximately 2.35 m) with 0.60 m RMSE. The high SWH areas in the mid-high latitudes of the Northern Hemisphere during January disappeared (Fig. 7a) with reduced overestimated bias (Fig.7b), whereas the SWHs in ACC became higher with the maximum bias of more than 3 m. In VR12-AL-ONLY experiments (Fig.6c&7c), compared with the CTRL, there are few differences, which indicates that the introducing of Langmuir mixing has little influence on wave state. Noticeably, in Z0-ONLY and VR12-AL-Z0 after introducing the wave-related z_0 to GFS, the overestimated biases have decreased, and in most regions the improvements are more than 5% (Fig.6d&e; Fig.7d&e). Compared Fig. 6b (7b) and Fig. 6d (7d), it is clear that the improvements mainly appear in regions where SWHs are overestimated, indicating that the wave-related z_0 can reduce the SWH. In VR12-AL-Z0-FAN (Fig.6f&7f), the z_0 from ST4-FAN parameterization (Fig. 2) has resulted in the global reduction of SWHs. As a result, the bias has decreased (increased) in areas where SWHs are overestimated (underestimated) in CTRL (Fig.6f&7f). The results in MS2K-Z0 are similar with that in VR12-AL-Z0 (Fig.6g&7g), and this again illustrates that the SWH simulation is not as sensitive to Langmuir mixing as to z_0.

https://doi.org/10.5194/gmd-2020-327
Preprint. Discussion started: 29 October 2020

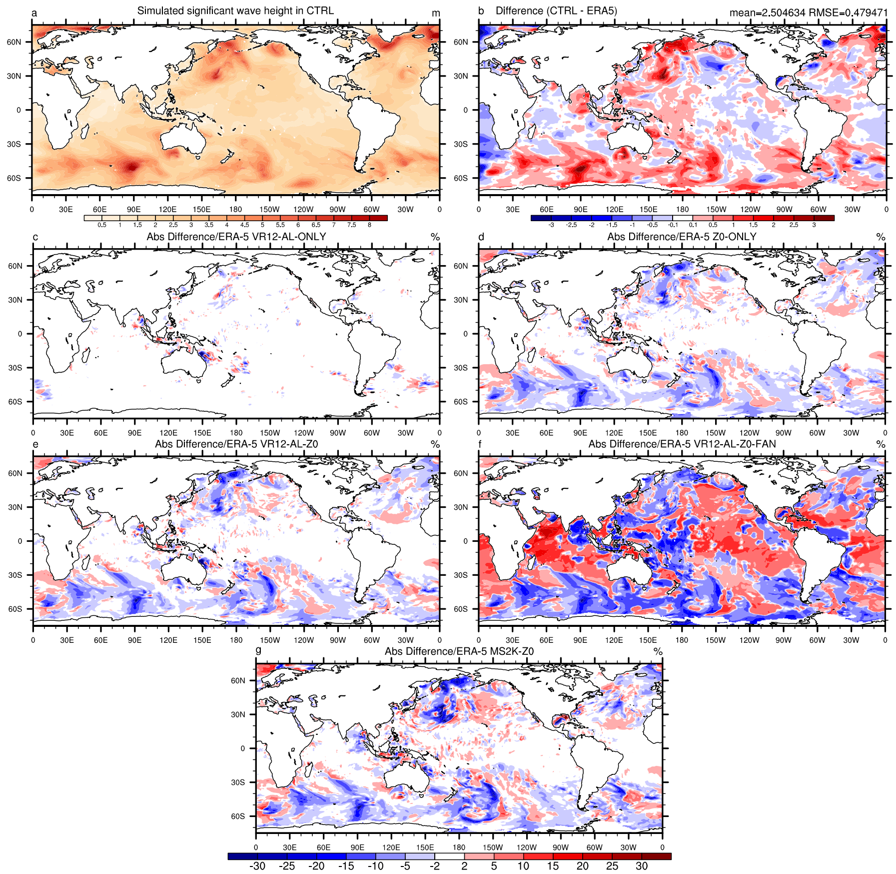

Figure 6. The SWH (m) in CTRL, its bias in CTRL and percentage absolute difference of bias on January 7, 2017: **a** the SWH in CTRL, **b** the SWH bias between CTRL and ERA5 (CTRL minus ERA5), **c/d/e/f/g** the percentage absolute difference between VR12-AL-ONLY/Z0-ONLY/VR12-AL-Z0/VR12-AL-Z0-FAN/MS2K-Z0 and CTRL. The absolute difference is a percentage computed as $\mathrm{PAD} = \frac{|\hat{y_s}-y|-|\hat{y_c}-y|}{|y|} \times 100\%$, where y is the SWH from ERA5, $\hat{y_c}$ is simulated SWH in CTRL and $\hat{y_s}$ is simulated SWH in other experiments, so a negative value means that the error is smaller than that of CTRL, and vice versa.

https://doi.org/10.5194/gmd-2020-327
Preprint. Discussion started: 29 October 2020

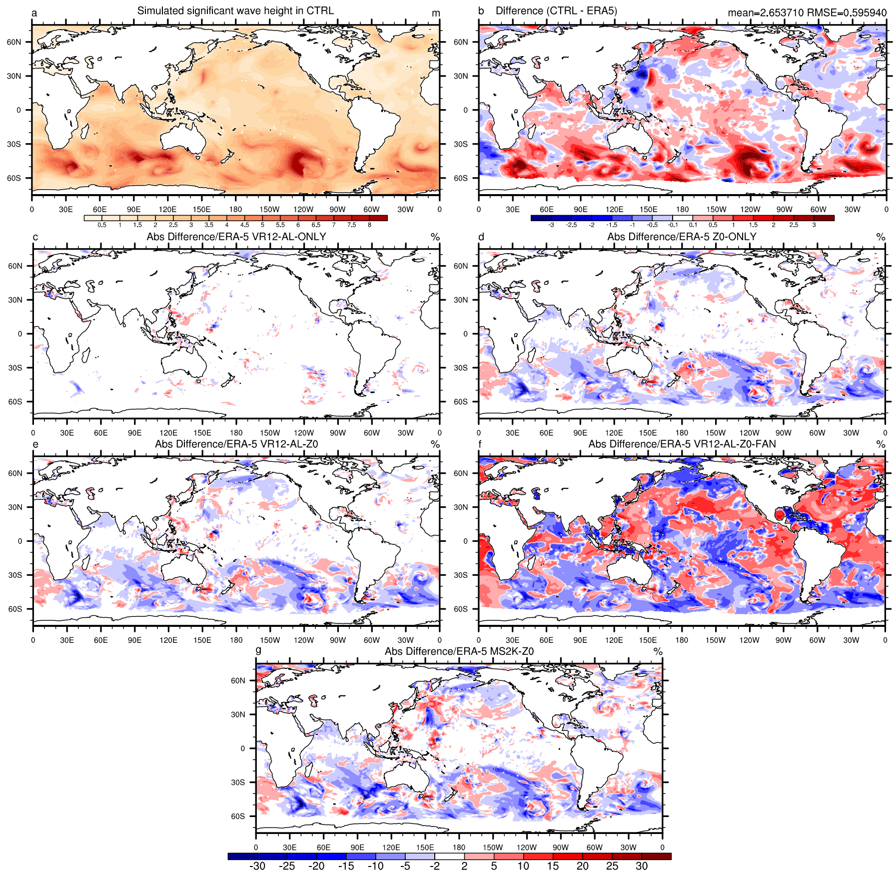

Figure 7. As Fig. 6, but for the SWH (m) in CTRL, its bias in CTRL and absolute difference of bias on August 7, 2018.

The waves in WW3 are mainly generated by the 10-m winds, since the effect of sea surface current is much weaker. The comparisons of the WSP10 from numerical experiments with the ERA5 wind data (Fig.8&9) indicate that the overestimated WSP10 (red shaded areas in Figs.8b&9b) could lead to the overestimated SWH (red shaded areas in Fig.6b&7b). In Z0-ONLY and VR12-AL-Z0 (Fig.8d&e; Fig.9d&e), after introduced the z_0 from ST4 in GFS, the biases of overestimated WSP10 are reduced and so are the biases of the SWH. In VR12-AL-Z0-FAN, the decrease of WSP10 is slightly weaker than those in VR12-AL-Z0 (Figs. 8f&9f), due to the z_0 from ST4-FAN which is lower than that from ST4

https://doi.org/10.5194/gmd-2020-327
Preprint. Discussion started: 29 October 2020

Geoscientific Model Development
Discussions
Open Access

at high winds (Fig. 2). With the combined effect of strong mixing and surface roughness in MS2K-Z0, the WSP10s decrease more (Figs.8g&9g). The similar SWH and WSP10 distributions at the last second (the 168th hour) are also shown in Figs. S3-S6 of the supplementary, with both the increase and decrease in biases due to the parameterizations becoming stronger. Moreover, the additional tests from January 1 to 8, 2019 and from July 1 to 8, 2018 also demonstrate the robustness of these results (Figs. S9-S12 in the supplementary).

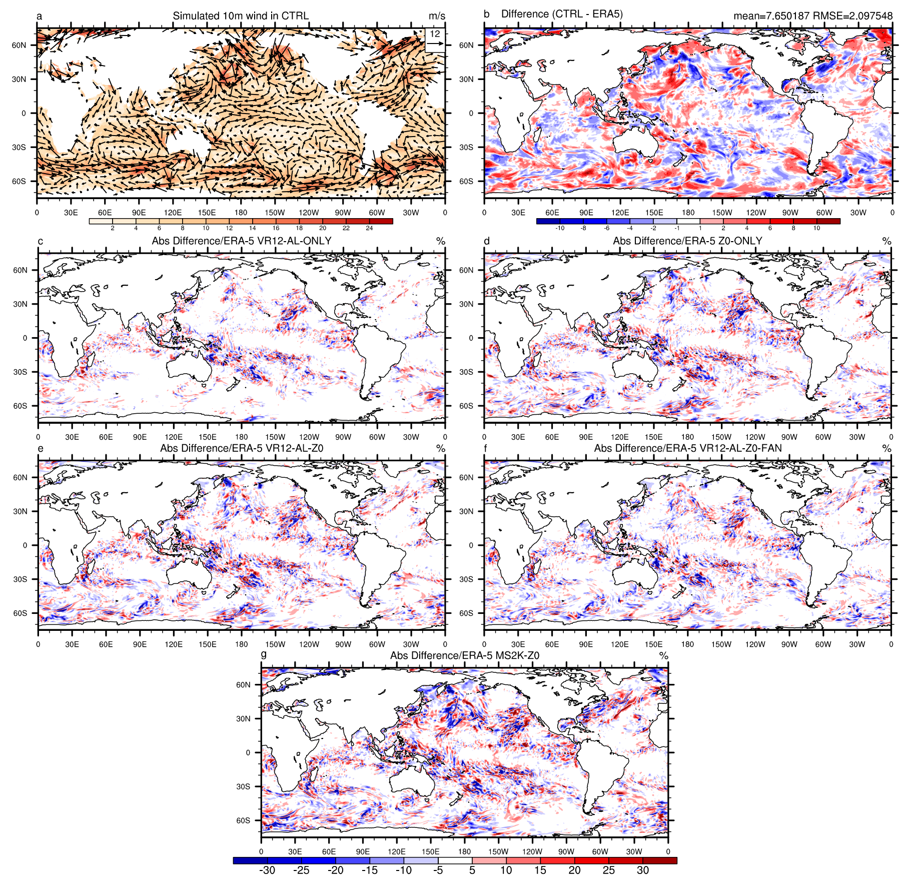

Figure 8. The WSP10 (m/s) in CTRL, its bias in CTRL and percentage absolute difference of bias on January 7, 2017: **a** the 10-m wind in CTRL, **b** the 10-m wind bias between CTRL and ERA5 (CTRL minus ERA5), **c/d/e/f/g** the percentage absolute difference between VR12-AL-ONLY/Z0-ONLY/VR12-AL-Z0/VR12-AL-Z0-FAN/MS2K-Z0 and CTRL. The absolute difference is a percentage computed as $\mathrm{PAD} = \frac{|\hat{y_s}-y|-|\hat{y_c}-y|}{|y|} \times 100\%$, where y is

https://doi.org/10.5194/gmd-2020-327
Preprint. Discussion started: 29 October 2020

WSP10 from ERA5, $\hat{y}_c$ is simulated WSP10 in CTRL and $\hat{y}_s$ is simulated WSP10 in other experiments, so a negative value means that the error is smaller than that of CTRL, and vice versa.

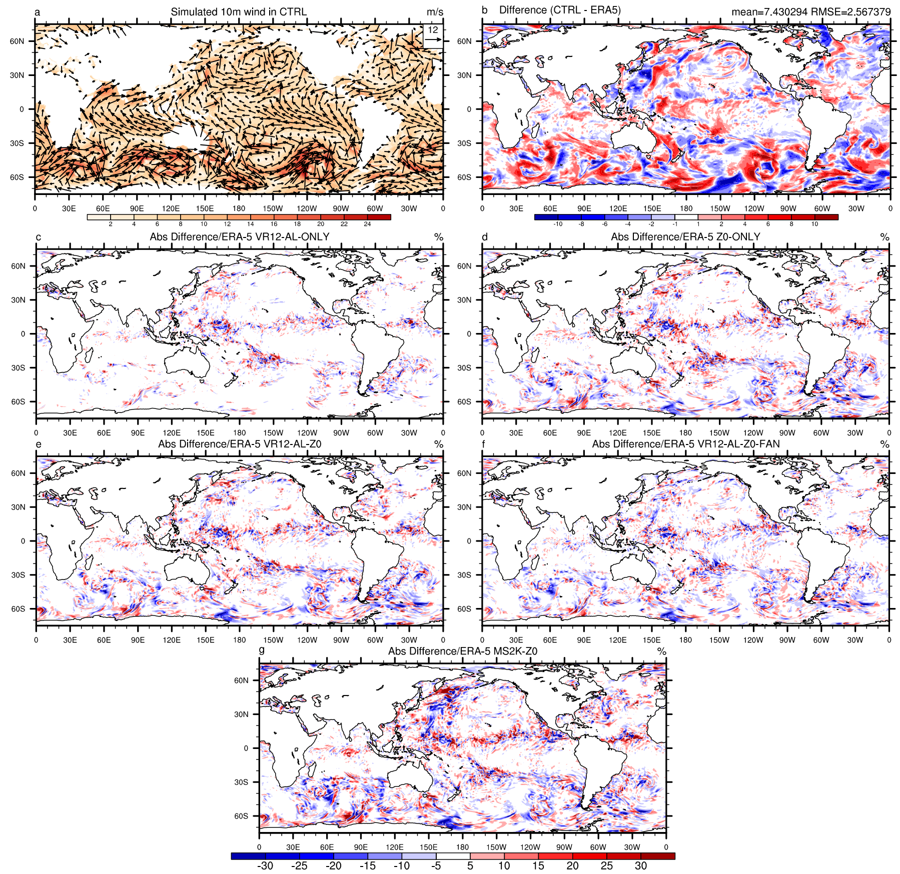

Figure 9. As Fig. 8, but for the WSP10 (m/s) in CTRL, its bias in CTRL and absolute difference of bias on August 7, 2018.

To demonstrate the relationship of SWH and WSP10 more clearly, we calculated the 7-day mean absolute percentage error (MAPE) for SWH and WSP10 between simulation results and NDBC buoy data (locations shown in Fig. 10). In general, the difference of SWH corresponds well to the difference of WSP between CTRL and ERA5 (shaded areas in Fig. 10). The lower the MAPE, the better the performance of the simulation. The corresponding MAPE differences compared with CTRL for the other

5 simulations are shown in Fig. 11, where a negative value means that the error is reduced versus CTRL and vice versa. From Fig. 11, it is clear that the distribution of MAPE for SWH (Fig. 11a&c) is in accordance with that for WSP10 (Fig. 11b&d). In the areas with overestimated SWH and WSP10, such as location 5 on January, 2017 (Fig. 10a&b) and location 3 on August, 2018 (Fig. 10c&d), after applying the wave-related z_0 in VR12-AL-Z0 and VR12-AL-Z0-FAN, the improvements of MAPEs are manifest for both SWH and WSP10 (Fig. 11). However, for the areas with underestimated SWH and WSP10, or with few biases, such as location 7, 8 on January, 2017 (Fig. 10a&b), the introduction of the wave-related z_0 slightly increases the MAPEs (Fig. 11a&b). Besides, although it has been indicated that the SWH is not sensitive to Langmuir mixing (Fig. 6c&7c), from Fig. 11 it is seen that as for the WSP10, VR12-AL-Z0 could perform better than Z0-ONLY, such as at location 10 on August, 2018 (Fig. 11d). This is probably because the enhanced turbulence kinetic energy in Langmuir mixing parameterization leads to more kinetic energy input from air to sea, which consequently results in the reduced surface wind speed.

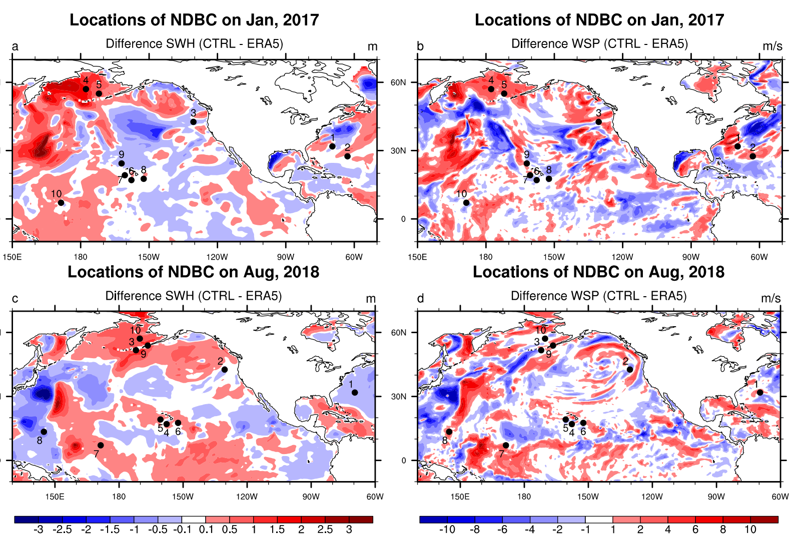

Figure 10. The locations of NDBC buoy data on Jan, 2017 (**a, b**) and Aug, 2018 (**c, d**); *Shaded* areas are SWH biases

https://doi.org/10.5194/gmd-2020-327
Preprint. Discussion started: 29 October 2020

(**a, c**) and WSP10 biases (**b, d**) between CTRL and ERA5 (CTRL minus ERA5).

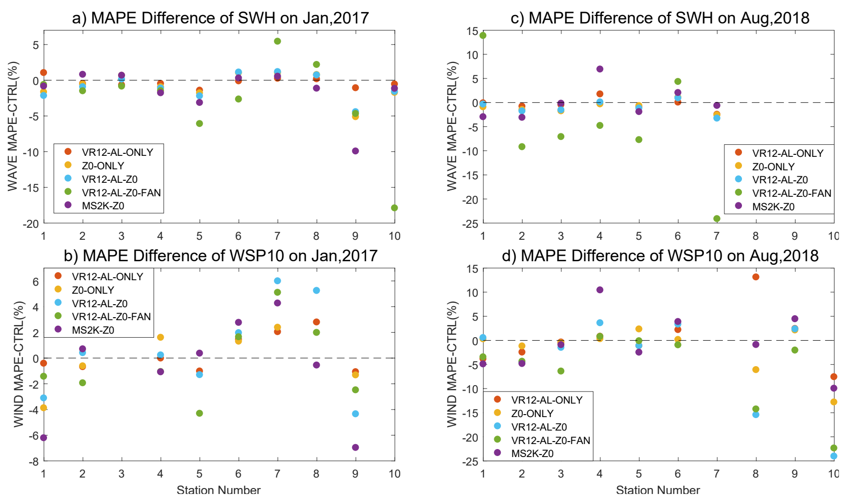

Figure 11. The mean absolute percentage error (MAPE) differences for SWH (**a, c**) and WSP10 (**b, d**) between VR12-AL-ONLY/Z0-ONLY/VR12-AL-Z0/VR12-AL-Z0-FAN/MS2K-Z0 and CTRL (MAPE in VR12-AL-ONLY/Z0-ONLY/VR12-AL-Z0/VR12-AL-Z0-FAN/MS2K-Z0 minus MAPE in CTRL) on Jan, 2017 (**a, b**) and Aug, 2018 (**c, d**); the MAPE is calculated as MAPE=$\left({100\%}/{n}\right)\sum_{i=1}^{n}\left|\frac{\hat{y}_i-y_i}{y_i}\right|$, where $\hat{y}_i$ is simulated value, y_i is NDBC buoy observation, i=1, 7; blank is missing value.

To understand the physical mechanism of how z_0 parameterization affect the SWH and WSP10, the scatterplot of various z_0 in ST4, ST4-FAN and original GFS need to be recalled (Fig. 2). The z_0 in WW3 with ST4 source term (purple dots) is larger than the original z_0 in GFS (black dots) at high wind speed (> 15m/s). The larger z_0 enhances frictional dissipation, therefore reduces the WSP10. And thus, the overestimated high WSP10s in CTRL are reduced in Z0-ONLY and VR12-AL-Z0. Furthermore, in regions like ACC, the overestimated WSP10s usually generate overestimated SWHs, therefore the reduced WSP10s could lead to the decrease of SWHs, and then improve the SWHs simulation in Z0-ONLY and VR12-AL-Z0. The ST4-FAN z_0 parameterization (dark red dots in Fig. 2) in VR12-AL-Z0-FAN has smaller z_0 at high wind speed than in ST4, however the generated z_0 at high wind (the threshold is less than ST4 and about 12m/s) is still larger than the original z_0 in GFS. Therefore, in

https://doi.org/10.5194/gmd-2020-327
Preprint. Discussion started: 29 October 2020

VR12-AL-Z0-FAN the reduction of the overestimated WSP10 in high wind areas is slightly weaker than that in VR12-AL-Z0, and so is the overestimated SWHs. Noticeably, the z_0 generated by ST4-FAN is larger than that generated by ST4 for WSP10 less than 15m/s, and enhances frictional dissipation, which could result in decreased SWHs at low winds. Thus, in VR12-AL-Z0-FAN the SWHs decrease globally, leading to reduced biases for overestimated SWHs but enhanced biases for underestimated SWHs.

5 Summary and Discussion

To investigate the role played by ocean surface gravity waves on atmosphere and ocean interface in a coupled global atmosphere-ocean-wave modeling system in a relatively short time range, we implemented the version 5.16 of WW3 to CFS2.0 for global oceans from 78°S-78°N, using the C-Coupler2. In this coupled system, the WW3 was forced by 10-m wind generated in GFS and sea surface current generated in MOM4. Langmuir mixing parameterizations, and momentum roughness length (z_0) parameterizations were applied and compared against in-situ buoys, satellite measurements and ERA5. The effects of waves on forecasting were examined in two winters and two summers. The results for the same season are consistent.

The following key results were found:

1. Langmuir mixing parameterizations could effectively reduce the SST and deepen MLD by generating strong vertical movements for 7-day forecasting. It is beneficial for areas with large errors of SST, such as the ACC. Particularly, the application of VR12-AL parameterization (Van et al. 2012) could significantly reduce the warm bias of SST and shallow bias of MLD in ACC in January, whereas its effects are nil in August. In contrast, the vertical mixing generated by MS2K parameterization is so strong that the SST is too cold and the MLD is too deep

https://doi.org/10.5194/gmd-2020-327
Preprint. Discussion started: 29 October 2020

compared with the observations.

2. With the application of ST4-FAN (Fan et al. 2012) for surface roughness length (z_0), z_0 becomes larger at high wind conditions, and leads to increased frictional dissipation at ocean-atmosphere interface. As a result, the overestimated wind speeds (usually in mid-high latitudes) are reduced. The reduced wind speeds subsequently decrease SWHs, and thus the overestimated SWHs produced by previously overestimated wind are also reduced.

As shown in Fig. 3, the Langmuir mixing induced SST improvements are mainly distributed in mid-high latitudes. SST biases also appeared in tropical oceans. In the work of Chune et al. (2018), the Nucleus for European Modelling of the Ocean (NEMO) model was one-way coupled with the Météo-France wave model (MFWAM) to refine the momentum as well as the energy flux across the air-sea interface. Consequently, the SST cold bias in the tropics is reduced. This offers a next direction to improve the global ocean forecast. Besides, some other processes such as nonbreaking wave-induced upper ocean mixing (Qiao et al., 2004), may also lead to improvements.

There still remain some biases in the coupled system, probably owing to the inaccuracy of coarse resolution, the incompleteness of direct wave-current interaction processes, and the deficiency of a unified assimilation system. In addition, to further improve the model and eliminate the biases, as Breivik et al. (2015) proposed, extra adjusting of the individual model components in the coupled systems is also necessary. All of these require further efforts to investigate efficient methods that can improve the ability of the fully coupled system.

Code and data availability

The code developed for the coupled system can be found under https://doi.org/10.5281/zenodo.4125726 (Shi et al., 2020), including the coupling, preprocessing, run control and postprocessing scripts. The initial fields for CFS are generated by the real time operational Climate Data Assimilation System, downloaded from the CFS official website (http://nomads.ncep.noaa.gov/pub/data/nccf/com/cfs/prod). The daily average satellite Optimum Interpolation SST (OISST) data are obtained from NOAA (https://www.ncdc.noaa.gov/oisst), and the National Data Buoy Center (NDBC) buoy data are also obtained from NOAA (https://www.ndbc.noaa.gov). The Argo observational profiles of temperature and salinity are available at China Argo Real-time Data Center (www.argo.org.cn). The ERA5 reanalysis are available at the Copernicus Climate Change Service (C3S) Climate Date Store (https://cds.climate.copernicus.eu/cdsapp#!/dataset/reanalysis-era5-single-levels). The along-track Jason-3 satellite data are obtained from AVISO CNES Data Center (https://aviso-data-center.cnes.fr).

Author contribution

FX and RS designed the experiments and RS carried them out. RS developed the code of coupling parametrizations and produced the figures. ZF contributed to the installation and operation of CFS2.0. LL and HY contributed to the application of C-Coupler2. XL and YZ provided the original code of CFS2.0. RS prepared the manuscript with contributions from all co-authors. FX contributed to review and editing.

Acknowledgments

The authors would like to extend thanks to all developers of the CFS2.0 model (https://cfs.ncep.noaa.gov/cfsv2/downloads.html). The work was supported by National Key Research and Development Program of China (no. 2016YFC1401408), and Tsinghua University Initiative Scientific Research Program (2019Z07L01001).

https://doi.org/10.5194/gmd-2020-327
Preprint. Discussion started: 29 October 2020

Geoscientific Model Development
Discussions

References

Ardhuin, F., Rogers, E., Babanin, A. V., Filipot, J., Magne, R., Roland, A., Der Westhuysen, A. V., Queffeulou, P., Lefevre, J. M., and Aouf, L.: Semiempirical Dissipation Source Functions for Ocean Waves. Part I: Definition, Calibration, and Validation, Journal of Physical Oceanography, 40, 1917-1941, http://dx.doi.org/10.1175/2010JPO4324.1, 2010.

Atlas, R., Hoffman, R. N., Ardizzone, J., Leidner, S. M., Jusem, J. C., Smith, D. K., and Gombos, D.: A Cross-calibrated, Multiplatform Ocean Surface Wind Velocity Product for Meteorological and Oceanographic Applications, Bulletin of the American Meteorological Society, 92, 157-174, http://dx.doi.org/10.1175/2010BAMS2946.1, 2011.

Belcher, S. E., Grant, A. L. M., Hanley, K., Foxkemper, B., Van Roekel, L., Sullivan, P. P., Large, W. G., Brown, A. R., Hines, A., and Calvert, D.: A global perspective on Langmuir turbulence in the ocean surface boundary layer, Geophysical Research Letters, 39, http://dx.doi.org/10.1029/2012GL052932, 2012.

Bidlot, J.-R.: Present status of wave forecasting at ECMWF, Workshop on ocean waves, 2012, 25-27.

Breivik, O., Mogensen, K., Bidlot, J., Balmaseda, M., and Janssen, P. A. E. M.: Surface wave effects in the NEMO ocean model: Forced and coupled experiments, Journal of Geophysical Research, 120, 2973-2992, http://dx.doi.org/10.1002/2014JC010565, 2015.

Charnock, H.: Wind stress on a water surface, Quarterly Journal of the Royal Meteorological Society, 81, 639-640, http://dx.doi.org/10.1002/qj.49708135027, 1955.

Chen, S. S., Price, J. F., Zhao, W., Donelan, M. A., and Walsh, E. J.: The CBLAST-Hurricane Program and the Next- Generation Fully Coupled Atmosphere-Wave-Ocean Models for Hurricane Research and

https://doi.org/10.5194/gmd-2020-327
Preprint. Discussion started: 29 October 2020

Prediction, Bulletin of the American Meteorological Society, 88, 311-317, http://dx.doi.org/10.1175/BAMS-88-3-311, 2007.

Chune, S. L., and Aouf, L.: Wave effects in global ocean modeling: parametrizations vs. forcing from a wave model, Ocean Dynamics, 68, 1739-1758, http://dx.doi.org/10.1007/s10236-018-1220-2, 2018.

de Boyer Montégut, C., Madec, G., Fischer, A. S., Lazar, A., and Iudicone, D.: Mixed layer depth over the global ocean: An examination of profile data and a profile-based climatology, Journal of Geophysical Research, 109, http://dx.doi.org/10.1029/2004JC002378, 2004.

Fan, Y., Lin, S., Held, I. M., Yu, Z., and Tolman, H. L.: Global Ocean Surface Wave Simulation Using a Coupled Atmosphere–Wave Model, Journal of Climate, 25, 6233-6252, http://dx.doi.org/10.1175/JCLI-D-11-00621.1, 2012.

Fan, Y., and Griffies, S. M.: Impacts of Parameterized Langmuir Turbulence and Nonbreaking Wave Mixing in Global Climate Simulations, Journal of Climate, 27, 4752-4775, http://dx.doi.org/10.1175/JCLI-D-13-00583.1, 2014.

Fox-Kemper, B., Adcroft, A., Boning, C. W., Chassignet, E. P., Curchitser, E. N., Danabasoglu, G., Eden, C., England, M. H., Gerdes, R., and Greatbatch, R. J.: Challenges and Prospects in Ocean Circulation Models, Frontiers in Marine Science, 6, 65, http://dx.doi.org/10.3389/fmars.2019.00065, 2019.

Griffies, S. M., Harrison, M. J., Pacanowski, R. C., and Rosati, A.: A technical guide to MOM4, GFDL Ocean Group Tech. Rep, 5, 342, 2004.

Hasselmann, K.: Wave-driven inertial oscillations, Geophysical and Astrophysical Fluid Dynamics, 1, 463-502, http://dx.doi.org/10.1080/03091927009365783, 1970.

Hersbach, H., and Dee, D.: ERA5 reanalysis is in production, ECMWF newsletter, 147, 5-6, 2016.

Janssen, P., and Janssen, P. A.: The interaction of ocean waves and wind, Cambridge University Press, 2004, pp 312.

Kalnay, E., Kanamitsu, M., Kistler, R., Collins, W. D., Deaven, D. G., Gandin, L. S., Iredell, M. D., Saha, S., White, G. H., and Woollen, J.: The NCEP/NCAR 40-Year Reanalysis Project, Bulletin of the American Meteorological Society, 77, 437-471, http://dx.doi.org/10.1175/1520-0477(1996)077%3C0437:TNYRP%3E2.0.CO;2, 1996.

Kohout, A. L., and Meylan, M. H.: An elastic plate model for wave attenuation and ice floe breaking in the marginal ice zone, Journal of Geophysical Research, 113, http://dx.doi.org/10.1029/2007JC004434, 2008.

Kukulka, T., Plueddemann, A. J., Trowbridge, J. H., and Sullivan, P. P.: Significance of Langmuir circulation in upper ocean mixing : comparison of observations and simulations, Geophysical Research Letters, 36, http://dx.doi.org/10.1029/2009GL037620, 2009.

Li, M., and Garrett, C.: Mixed Layer Deepening Due to Langmuir Circulation, Journal of Physical Oceanography, 27, 121-132, http://dx.doi.org/10.1175/1520-0485(1997)027%3C0121:MLDDTL%3E2.0.CO;2, 1997.

Li, Q., Webb, A., Foxkemper, B., Craig, A., Danabasoglu, G., Large, W. G., and Vertenstein, M.: Langmuir mixing effects on global climate: WAVEWATCH III in CESM, Ocean Modelling, 103, 145-160, http://dx.doi.org/10.1016/j.ocemod.2015.07.020, 2016.

Li, Q., Foxkemper, B., Breivik, O., and Webb, A.: Statistical models of global Langmuir mixing, Ocean Modelling, 113, 95-114, http://dx.doi.org/10.1016/j.ocemod.2017.03.016, 2017.

Li, Z., Liu, Z., & Xing, X.: User Manual for Global Argo Observational data set (V3.0) (1997-2019), China Argo Real-time Data Center, Hangzhou, 37pp, 2019.

https://doi.org/10.5194/gmd-2020-327
Preprint. Discussion started: 29 October 2020

Geoscientific Model Development Discussions
Open Access EGU

Liu, L., Zhang, C., Li, R., and Wang, B.: C-Coupler2: a flexible and user-friendly community coupler for model coupling and nesting, Geoscientific Model Development Discussions, 11, 1-63, http://dx.doi.org/10.5194/gmd-11-3557-2018, 2018.

Mcwilliams, J. C., and Sullivan, P. P.: Vertical Mixing by Langmuir Circulations, Spill Science & Technology Bulletin, 6, 225-237, http://dx.doi.org/10.1016/S1353-2561(01)00041-X, 2000.

Moon, I., Ginis, I., and Hara, T.: Effect of surface waves on Charnock coefficient under tropical cyclones, Geophysical Research Letters, 31, http://dx.doi.org/10.1029/2004GL020988, 2004.

Moum J.N., and Smyth W.D.: Upper Ocean Mixing. In Cochran, J. Kirk; Bokuniewicz, J. Henry; Yager, L. Patricia (Eds.) Encyclopedia of Ocean Sciences, 3rd Edition. vol. 1, pp. 71-79, Elsevier. ISBN: 978-0-12-813081-0, 2019.

Pianezze, J., Barthe, C., Bielli, S., Tulet, P., Jullien, S., Cambon, G., Bousquet, O., Claeys, M., and Cordier, E.: A New Coupled Ocean-Waves-Atmosphere Model Designed for Tropical Storm Studies: Example of Tropical Cyclone Bejisa (2013–2014) in the South-West Indian Ocean, Journal of Advances in Modeling Earth Systems, 10, 801-825, http://dx.doi.org/10.1002/2017MS001177, 2018.

Prakash, K. R., Nigam, T., and Pant, V.: Estimation of oceanic subsurface mixing under a severe cyclonic storm using a coupled atmosphere–ocean–wave model, Ocean Science, 14, 259-272, http://dx.doi.org/10.5194/os-14-259-2018, 2018.

Qiao, F., Yuan, Y., Yang, Y., Zheng, Q., Xia, C., and Ma, J.: Wave-induced mixing in the upper ocean: Distribution and application to a global ocean circulation model, Geophysical Research Letters, 31, http://dx.doi.org/10.1029/2004GL019824, 2004.

https://doi.org/10.5194/gmd-2020-327
Preprint. Discussion started: 29 October 2020

Geoscientific Model Development Discussions

Qiao, F., Yuan, Y., Ezer, T., Xia, C., Yang, Y., Lu, X., and Song, Z.: A three-dimensional surface wave–ocean circulation coupled model and its initial testing, Ocean Dynamics, 60, 1339-1355, http://dx.doi.org/10.1007/s10236-010-0326-y, 2010.

Reynolds, R. W., Smith, T. M., Liu, C., Chelton, D. B., Casey, K. S., and Schlax, M. G.: Daily High-Resolution-Blended Analyses for Sea Surface Temperature, Journal of Climate, 20, 5473-5496, http://dx.doi.org/10.1175/2007JCLI1824.1, 2007.

Ricchi, A., Miglietta, M. M., Barbariol, F., Benetazzo, A., Bergamasco, A., Bonaldo, D., Cassardo, C., Falcieri, F. M., Modugno, G., and Russo, A.: Sensitivity of a Mediterranean Tropical-Like Cyclone to Different Model Configurations and Coupling Strategies, Atmosphere, 8, 92, http://dx.doi.org/10.3390/atmos8050092, 2017.

Saha, S., Moorthi, S., Pan, H., Wu, X., Wang, J., Nadiga, S., Tripp, P., Kistler, R., Woollen, J., and Behringer, D.: The NCEP Climate Forecast System Reanalysis, Bulletin of the American Meteorological Society, 91, 1015-1057, http://dx.doi.org/10.1175/2010BAMS3001.1, 2010.

Saha, S., Moorthi, S., Wu, X., Wang, J., Nadiga, S., Tripp, P., Behringer, D., Hou, Y., Chuang, H., and Iredell, M. D.: The NCEP Climate Forecast System Version 2, Journal of Climate, 27, 2185-2208, http://dx.doi.org/10.1175/JCLI-D-12-00823.1, 2014.

Squire, V. A., Vaughan, G. L., and Bennetts, L. G.: Ocean surface wave evolvement in the Arctic Basin, Geophysical Research Letters, 36, http://dx.doi.org/10.1029/2009GL040676, 2009.

Stopa, J. E., Ardhuin, F., Babanin, A. V., and Zieger, S.: Comparison and validation of physical wave parameterizations in spectral wave models, Ocean Modelling, 103, 2-17, http://dx.doi.org/10.1016/j.ocemod.2015.09.003, 2016.

Sun, J., Wei, Z., Xu, T., Sun, M., Liu, K., Yang, Y., Chen, L., Zhao, H., Yin, X., and Feng, W.: Development of a fine-resolution atmosphere-wave-ocean coupled forecasting model for the South China Sea and its adjacent seas, Acta Oceanologica Sinica, 38, 154-166, http://dx.doi.org/10.1007/s13131-019-1419-1, 2019.

Taylor, P. K., and Yelland, M. J.: The Dependence of Sea Surface Roughness on the Height and Steepness of the Waves, Journal of Physical Oceanography, 31, 572-590, http://dx.doi.org/10.1175/1520-0485(2001)031%3C0572:TDOSSR%3E2.0.CO;2, 2001.

Terray, E. A., Donelan, M. A., Agrawal, Y. C., Drennan, W. M., Kahma, K. K., Williams, A. J., Hwang, P. A., and Kitaigorodskii, S. A.: Estimates of Kinetic Energy Dissipation under Breaking Waves, Journal of Physical Oceanography, 26, 792-807, http://dx.doi.org/10.1175/1520-0485(1996)026%3C0792:EOKEDU%3E2.0.CO;2, 1996.

Tolman, H. L., and Chalikov, D. V.: Source Terms in a Third-Generation Wind Wave Model, Journal of Physical Oceanography, 26, 2497-2518, http://dx.doi.org/10.1175/1520-0485(1996)026%3C2497:STIATG%3E2.0.CO;2, 1996.

Van Roekel, L. P., Foxkemper, B., Sullivan, P. P., Hamlington, P. E., and Haney, S.: The form and orientation of Langmuir cells for misaligned winds and waves, Journal of Geophysical Research, 117, http://dx.doi.org/10.1029/2011JC007516, 2012.

Warner, J. C., Armstrong, B., He, R., and Zambon, J. B.: Development of a Coupled Ocean-Atmosphere-Wave-Sediment Transport (COAWST) Modeling System, Ocean Modelling, 35, 230-244, http://dx.doi.org/10.1016/j.ocemod.2010.07.010, 2010.

WAVEWATCH III Development Group.: User manual and system documentation of WAVEWATCH III version 5.16, NOAA/NWS/NCEP/MMAB Technical Note 329, 326, 2016.

Wu, Z., Jiang, C., Chen, J., Long, Y., Deng, B., and Liu, X.: Three-Dimensional Temperature Field Change in the South China Sea during Typhoon Kai-Tak (1213) Based on a Fully Coupled Atmosphere–Wave–Ocean Model, Water, 11, 140, http://dx.doi.org/10.3390/w11010140, 2019.

Zieger, S., Babanin, A. V., Rogers, W. E., and Young, I. R.: Observation-based source terms in the third-generation wave model WAVEWATCH, Ocean Modelling, 96, 2-25, http://dx.doi.org/10.1016/j.ocemod.2015.07.014, 2015.